Wang *et al. Chem Synth* 2024;4:34
DOI: 10.20517/cs.2024.24

Chemical Synthesis

Research Article

Open Access

Check for updates

A 3D ordered hierarchical crystalline porous organic salt for large-sized enzyme immobilization

Jinman Wang[1], Guolong Xing[1,2,3,*], Yu Zhao[1,3], Jinming Zhou[3], Bo Song[2,4], Li-Hua Chen[5], Weidong Zhu[1,3], Bao-Lian Su[5,6,*], Teng Ben[1,2,3,*]

[1]Zhejiang Engineering Laboratory for Green Syntheses and Applications of Fluorine-Containing Specialty Chemicals, Institute of Advanced Fluorine-Containing Materials, Zhejiang Normal University, Jinhua 321004, Zhejiang, China.
[2]Science and Technology Center for Quantum Biology, National Institute of Extremely-Weak Magnetic Field Infrastructure, Hangzhou 310000, Zhejiang, China.
[3]Key Laboratory of the Ministry of Education for Advanced Catalysis Materials, Institute of Physical Chemistry, Zhejiang Normal University, Jinhua 321004, Zhejiang, China.
[4]School of Optical-Electrical Computer Engineering, University of Shanghai for Science and Technology, Shanghai 200093, China.
[5]Laboratory of Living Materials at the State Key Laboratory of Advanced Technology for Materials Synthesis and Processing, Wuhan University of Technology, Wuhan 430070, Hubei, China.
[6]Laboratory of Inorganic Materials Chemistry, University of Namur, Namur B-5000, Belgium.

[*]**Correspondence to:** Dr. Guolong Xing, Prof. Teng Ben, Zhejiang Engineering Laboratory for Green Syntheses and Applications of Fluorine-Containing Specialty Chemicals, Institute of Advanced Fluorine-Containing Materials, Zhejiang Normal University, Yingbin Road 688, Jinhua 321004, Zhejiang, China. E-mail: xinggl@zjnu.edu.cn; tengben@zjnu.edu.cn; Prof. Bao-Lian Su, Laboratory of Inorganic Materials Chemistry, University of Namur, Rue de Bruxelles 61, Namur B-5000, Belgium. E-mail: bao-lian.su@unamur.be

How to cite this article: Wang J, Xing G, Zhao Y, Zhou J, Song B, Chen LH, Zhu W, Su BL, Ben T. A 3D ordered hierarchical crystalline porous organic salt for large-sized enzyme immobilization. *Chem Synth* 2024;4:34. https://dx.doi.org/10.20517/cs.2024.24

Received: 26 Feb 2024 **First Decision:** 20 Mar 2024 **Revised:** 16 Apr 2024 **Accepted:** 28 May 2024 **Published:** 12 Jun 2024

Academic Editors: Wei Li, Yi Tang, Ying Wan **Copy Editor:** Pei-Yun Wang **Production Editor:** Pei-Yun Wang

Abstract

Crystalline porous organic salts (CPOSs) are an emerging class of promising materials with intrinsic highly polar nanoconfined microporosity. However, their single microporous structure greatly hinders their development in the field of catalysis and adsorption. Constructing a hierarchical porous structure can effectively reduce the mass transport resistance, thus expanding the scope of their applications. Herein, we report the synthesis of a three-dimensional (3D) ordered macro-/microporous hierarchical CPOS (HCPOS-1) using a template-assisted approach for the first time. The as-synthesized HCPOS-1 prepared from a polystyrene colloidal crystal template showcases a 3D ordered macroporous structure while also preserving the microporous structure. The 3D ordered macroporous structure in such a hierarchical structure, together with its hydrophilic surface, endows HCPOS-1 with the ability to

immobilize large-sized enzymes through physical adsorption under mild conditions. The resulting catalase/HCPOS-1 showcases a high enzyme immobilization capacity and avoids undesired conformational changes of enzymes during the immobilization process, thus exhibiting excellent catalytic activity for the decomposition of hydrogen peroxide.

Keywords: Crystalline porous organic salts, hierarchical pores, template-assisted method, enzyme immobilization, catalysis

INTRODUCTION

Crystalline porous organic salts (CPOSs), as a novel class of porous organic materials constructed from organic acids and organic bases via ionic bonding, have aroused significant attention and made notable advancements in diverse fields[1,2]. Although the micropores in their structure endow them with an impressive micropore surface area, the single microporous structure impedes mass transfer and severely restricts their further application in catalysis, adsorption, and various other fields[3-15]. Hierarchical porous structures composed of interconnecting pores with different sizes widely exist in nature, which maximize the efficiency of substance transport and reaction rate, and ensure efficient chemical reactions in organisms[16-18]. Introducing hierarchical porous structures into CPOSs is conducive to reducing mass transfer resistance and accommodating larger molecules than micropores, thus expanding the scope of application for CPOSs[2]. Nevertheless, synthesizing CPOSs with hierarchical porous structures remains an enormous challenge due to the rapid reaction rate and flexible bonding motifs of organic acids and bases.

The template-assisted technique represents a highly effective strategy for fabricating exquisite hierarchical porous materials[19]. By employing this method, the pore size of resulting hierarchical porous materials can be finely tuned over a wide range, depending on the dimensions of the chosen template. Furthermore, compared to alternative approaches such as elongated ligands, this technique offers a more streamlined and less challenging synthetic process for fabricating hierarchical porous materials[20]. Currently, the template-assisted method has gained significant traction in fabricating hierarchical porous materials and has been successfully applied to fabricating hierarchical crystalline porous materials such as metal- (MOFs) and covalent organic frameworks (COFs)[21-26]. In 2018, Shen *et al.* first prepared three-dimensional (3D) ordered micro-/microporous MOF single crystals utilizing polystyrene (PS) colloidal crystal as the sacrifice template[21]. More recently, Liu *et al.* successfully employed this methodology to prepare ordered macro-/microporous single crystals of COFs under solvothermal conditions with aniline as the modulator[26]. Notably, selecting the synthesis conditions requires careful consideration, as the solvent should be incompatible with the template and the reaction conditions should have negligible impact on the structural integrity of the template. The synthesis conditions employed for CPOSs are relatively mild compared to the harsh synthesis conditions (e.g., high temperature, pressure, *etc.*) typically associated with COFs and MOFs. Furthermore, the solvents predominantly employed in fabricating CPOSs are primarily aqueous or alcoholic in nature, imparting minimal influence on the template. Consequently, the template-assisted method holds great promise for facilitating the preparation of CPOSs featuring hierarchical porous structures. Notably, the elaborately engineered hierarchical CPOSs (HCPOS) may have a potential application in the adsorption of large guest molecules.

Enzymes, as natural catalysts, facilitate highly efficient and specific catalysis under mild conditions[27,28]. Immobilizing enzymes within porous materials represents a potent approach to expand their applications[29-43]. Nevertheless, the size of enzymes typically exceeds the micropore dimensions of porous materials. This discrepancy becomes even more pronounced for large-sized enzymes, presenting persistent challenges for their immobilization. Although *in-situ* encapsulation can immobilize large-sized enzymes

within porous materials, the interactions between the building blocks, organic solvents, and harsh synthesis conditions during the immobilization process often lead to decreased or even loss of enzyme activity[44,45]. Alternatively, the physical adsorption strategy, which allows for enzyme immobilization under mild conditions, emerges as a favorable option[46,47]. Hierarchical porous materials with an appropriate pore size endow them with the ability to immobilize large-sized enzymes. The large pore ensures sufficient space for effective mass transfer and the preservation of enzyme's freedom, while the small pore guarantees a high surface area for adsorbing more substrates. Compared to hierarchical MOFs and COFs, CPOSs with a hierarchical porous structure have hydrophilic surfaces and no toxic metal ions, rendering them an ideal platform for immobilizing large-sized enzymes. To the best of our knowledge, there have been no reports on the immobilization of large-sized enzymes using HCPOSs.

Herein, we report, for the first time, a template-assisted method for preparing a 3D ordered HCPOS. CPOS-1, self-assembly from tetrakis(4-sulfophenyl)methane (TSPM) and *trans*-1,4-diaminocyclohexane (DACH) via ionic bond, is selected, as a proof of concept. PS nanosphere colloidal crystals are applied as the sacrifice template and enabled the *in-situ* growth of CPOS-1 within the ordered voids. The obtained HCPOS-1 demonstrates a 3D ordered macroporous structure and also retains the crystallinity, microporous, and stability nature of CPOS-1. Intriguingly, the abundant macropores enable HCPOS-1 to immobilize large-sized enzyme [catalase (CAT)] under mild conditions with a high immobilization capacity of 336.9 $mg \cdot g^{-1}$, which surpasses CPOS-1 and many other porous organic materials. Furthermore, CAT/HCPOS-1 exhibits excellent catalytic activity for decomposing hydrogen peroxide (H_2O_2) due to the preservation of enzyme conformation during the immobilization process. These research findings provide a clear case for preparing HCPOSs while also offering useful insights for the immobilization of large-sized enzymes.

EXPERIMENTAL

Materials

Styrene and polyvinylpyrrolidone (K29-32, M_w = 58,000, PVP) were purchased from J&K Scientific (Beijing, China). Chlorosulfonic acid ($ClSO_3H$) was purchased from Energy Chemical (Shanghai, China). DACH was purchased from TCI (Shanghai, China). CAT (EC 1.11.1.6 from bovine liver, 2,000-5,000 units/mg protein) was purchased from Sigma-Aldrich (USA). Fluorescein isothiocyanate (FITC), ammonium iron (II) sulfate and 2-methyl-imidazole (HmIM) were purchased from Bide (Shanghai, China). $Zn(OAc)_2 \cdot 2H_2O$ was purchased from Dongnan Chemical (Jinhua, China). Bradford assay kit was purchased from Bioss (Shanghai, China). H_2O_2 (1 M) was purchased from Beyotime (Shanghai, China). Sorbitol was purchased from Macklin (Shanghai, China). Xylenol Orange sodium salt and potassium persulfate ($K_2S_2O_8$, KPS) were purchased from Mreda (Beijing, China). Tris-HCl buffer (50 mM, pH 8) and phosphate-buffered saline (PBS) buffer (50 mM, pH 7) were obtained from Yuanye (Shanghai, China). All chemicals and solvents were used as received without further purification.

Synthesis of 3D ordered polystyrene colloidal crystal template

The PS template was prepared according to the previous literature reported by Shen *et al.*[21]. Styrene was first washed thoroughly with 10 wt.% NaOH solution and deionized water to remove the stabilizer. Then, 32.5 mL styrene was added to 250.0 mL deionized water containing 1.25 g PVP. After bubbling with nitrogen for 30 min, the mixture was stirred at 75 °C for 30 min. Subsequently, 25.0 mL of $K_2S_2O_8$ (0.02 $g \cdot mL^{-1}$) was quickly added to initiate the reaction. After stirring for 24 h at this temperature, the obtained milk-like product was the monodispersed colloidal PS spheres.

The formation of 3D ordered PS colloidal crystal template from monodisperse PS was easily achieved by filtration. The colloidal dispersions of PS were carefully poured onto a filter funnel pre-setted with three conventional filter papers under vacuum. After three days, burly filter cakes were formed, which were further washed with deionized water and dried at 80 °C overnight.

Synthesis of CPOS-1-Cryst

CPOS-1 crystals (CPOS-1-Cryst) were prepared according to previous literature with some modifications[3]. First, 21.4 mg TSPM (0.025 mmol) was dissolved in 3.0 mL methanol and 1.0 mL H_2O. Then, 5.7 mg DACH (0.050 mmol) was dissolved in 3.0 mL methanol and 1.0 mL H_2O. The obtained solutions were filtered and mixed. The mixture was allowed to stand at room temperature overnight to obtain CPOS-1-Cryst as a light-yellow crystal (13.4 mg, 71.3%).

Synthesis of HCPOS-1

First, 5.7 mg DACH (0.050 mmol) was dissolved in 1.5 mL absolute methanol. Next, a 2.0-3.0 g PS template was immersed in the solution of DACH for 4 h. Then, the methanol was removed under vacuum at room temperature for 2 h to obtain DACH@PS. In a separate step, 21.4 mg TSPM (0.025 mmol) was dissolved in 6.0 mL methanol and 2.0 mL H_2O. The DACH@PS was immersed in the TSPM solution overnight. Subsequently, vacuum at room temperature for 3 h, and then immersed in tetrahydrofuran (THF) for 24 h to remove the PS template. Finally, the resultant was washed by THF and dried at 150 °C for 8 h to give HCPOS-1 (12.2 mg, 64.7%).

Synthesis of CPOS-6

CPOS-6 was prepared according to the previous literature[6]. First, 10.3 mg TSPM (0.012 mmol) was dissolved in 1.2 mL methanol. Next, 7.2 mg tetrakis(4-amidinophenyl)methane hydrochloride (TAmPM, 0.012 mmol) was dissolved in 1.45 mL H_2O. The obtained solutions were filtered and mixed. The mixture was allowed to stand at room temperature overnight to obtain CPOS-6 as a light-yellow crystal (6.8 mg, 46.6%).

Synthesis of HCPOS-6

First, 20.6 mg TSPM (0.024 mmol) was dissolved in 1.5 mL methanol. Next, 4.0-5.0 g PS template was immersed in the TSPM solution for 4 h; then, the methanol was removed under vacuum at room temperature for 2 h to obtain TSPM@PS. Subsequently, 14.4 mg TAmPM (0.025 mmol) was dissolved in 2.4 mL methanol and 2.9 mL H_2O. The TSPM@PS was immersed in the TAmPM solution overnight, then vacuum at room temperature for 3 h, and immersed in THF for 24 h to remove the PS template. Finally, the resultant was washed by THF and dried at 150 °C for 8 h to yield HCPOS-6 (7.9 mg, 27.0%).

Synthesis of ZIF-8

Zeolitic imidazolate framework (ZIF)-8 was synthesized according to a previous report with some modifications[48]. First, 526.0 mg $Zn(OAc)_2{\cdot}2H_2O$ (2.4 mmol) was dissolved in 20.0 mL H_2O, and 3.15 g HmIM (38.4 mmol) was dissolved in 20.0 mL H_2O. Then, the above-obtained solutions were mixed. The reaction mixture was left under stirred conditions at room temperature. After 24 h, the precipitate was collected by filtration and dried at 80 °C overnight (0.56 g, 96.1%).

Synthesis of fluorescein-tagged CAT/HCPOS-1

Fluorescein-tagged CAT (FCAT) was prepared according to a previous report with some modifications[49]. First, 10.0 mg CAT was dissolved in carbonate-bicarbonate aqueous buffer solution (0.1 M, pH 9, 2.0 mL). Then, 5.0 mg FITC was dissolved in 1.0 mL dimethyl sulfoxide (DMSO). After mixing CAT and FITC solution and stirring for 2 h without light at room temperature, the unreacted FITC was removed by

washing with ethanol and ultrapure water. Subsequently, 20.0 mg HCPOS-1 was added into FCAT solution and stirred overnight; the FCAT/HCPOS-1 was obtained by centrifugation at 18,000 rpm for 3 min and then washed, sonicated, and centrifuged in ultrapure water three times.

Synthesis of CAT/HCPOS-1

First, 3.0 mg HCPOS-1 was added into 2.0 mL CAT aqueous solution (2 $mg \cdot mL^{-1}$, centrifugated at 12,000 rpm for 10 min); the mixture was left under static conditions at 8 °C for 6 h. CAT/HCPOS-1 was obtained by filtration.

Synthesis of CAT/ZIF-8

First, 3.0 mg ZIF-8 was added into 2.0 mL CAT aqueous solution (2 $mg \cdot mL^{-1}$, centrifugated at 12,000 rpm for 10 min); the mixture was left under static conditions at 8 °C for 6 h. CAT/ZIF-8 was obtained by filtration.

Characterizations

^{1}H nuclear magnetic resonance (NMR) was recorded on Bruker 400 MHz NMR spectrometer. Tecan infinite 200Pro microplate reader was used to record the catalytic process. The powder X-ray diffraction (PXRD) patterns of all materials were collected on a Bruker D8 Advance instrument with Cu-Kα radiation operating at 40 kV and 40 mA, and recorded from 2° to 40° (2θ) at a scan rate of 0.1 time/step. The thermogravimetric analysis (TGA) data was collected on a Netzsch STA 449 C analyzer at a heating rate of 10 $°C \cdot min^{-1}$ ranging from 30-900 °C under air atmosphere. Fourier transform infrared (FT-IR) spectra of all materials were obtained on a Nicolet iS50 FT-IR spectrometer using approximately 3 mg of ground sample. In this work, an attenuated total reflectance (ATR) sampling tool was used for the FT-IR test. Sixty-four scans were recorded over the range of 4,000-400 cm^{-1}. Gas adsorption isotherms were obtained on ASAP 2020. Approximately 50 mg of the sample was placed into a glass analysis tube and degassed under dynamic vacuum for 8 h at 150 °C before measurement. The carbon dioxide (CO_2) adsorption-desorption analysis was conducted at 273 K. The confocal laser scanning microscopy (CLSM) image was collected on Carl Zeiss LSM 880 under an excitation of 488 nm. Scanning electron microscopy (SEM) was performed on Carl Zeiss Gemini SEM 300 with 5 kV and Hitachi S-4800 SEM with 10 kV. Transmission electron microscopy (TEM) was performed on JEOL JEM2100 at an operating voltage of 200 kV. Samples were dispersed with ethanol and dripped onto a 200 mesh copper net. The ultraviolet-visible (UV-vis) spectra were attained with a Shimadzu UV-2700 spectrometer. The circular dichroism (CD) measurements were obtained using a MOS-500 Spectrometer. Samples were measured using a 1.0 cm path length cuvette. The spectra were recorded from 220 to 260 nm with a path length of 2.0 nm. Water contact angle was measured using a SINDIN SDC-100 optical contact angle tension measuring instrument (Dongguan). Surface hydrophobicity/hydrophilicity was evaluated by measuring the contact angles between sessile water droplets and materials.

Determination of the immobilization capacity of enzyme

The enzyme amounts in solution before and after the immobilization measured with the Bradford method[50,51].

$$\text{Enzyme immobilization capacity} = (C_1 - C_2)V/m$$

Here, C_1 and C_2 (mg/mL) mean the CAT concentration before and after immobilization; V (mL) is the volume of the CAT aqueous solution, and m (mg) represents the mass of material initially added to the solution.

Catalytic performance of CAT/HCPOS-1 and CAT/ZIF-8 Composites

The ferrous oxidation in the xylenol orange (FOX) assay was applied to quantify the H_2O_2 concentration[52,53]. The concentration of the commercial H_2O_2 standard was first calculated spectrophotometrically at 240 nm with $\varepsilon = 39.4\ M^{-1}\cdot cm^{-1}$. The desired mass of CAT/HCPOS-1 or CAT/ZIF-8 was added into Tris-HCl buffer (50 mM, pH 8, 500 μL). Thereafter, 500 μL H_2O_2 stock solution was added. At different time intervals, 50 μL aliquots of the mixtures were sampled and mixed with 950 μL of FOX reagent in a centrifugal tube and then incubated for at least 30 min at room temperature. After incubation, the samples were centrifuged. The absorbance value at 560 nm for the supernatant was recorded to calculate the H_2O_2 concentration.

Storage stability of CAT/HCPOS-1

The storage stability of CAT/HCPOS-1 was determined by incubating them at -20 °C, and tested the activity every seven days with 1.5 mg CAT/HCPOS-1 and 0.25 mM H_2O_2.

RESULTS AND DISCUSSION

A 3D ordered HCPOS was meticulously synthesized employing a template-assisted method in the presence of a PS colloid crystal template, as illustrated in Figure 1. Considering the stability of CPOS and the influence of synthetic solvents on the template during the synthesis process, CPOS-1, self-assembled from TSPM and DACH through ionic bonding in methanol, was chosen as an example for the HCPOS synthesis. In order to fabricate a magnificent HCPOS-1, we synthesized large CPOS-1 crystals, denoted as CPOS-1-Cryst, according to the previous report with some modifications[3]. CPOS-1-Cryst was synthesized from TSPM and DACH by an acid-base reaction in a mixture of methanol/H_2O (3/1, v/v). Adding H_2O slows the reaction rate between TSPM and DACH and prolongs the precipitation time of crystals, thereby forming large CPOS-1 crystals [Supplementary Figure 1]. The structure of the as-synthesized CPOS-1-Cryst was confirmed through characterization techniques (e.g., ^{1}H NMR, FT-IR, PXRD, *etc.*), consistent with previous reports [Supplementary Figures 2-4]. Subsequently, uniformly sized and monodisperse PS nanospheres were prepared using established methods, and a 3D ordered PS colloidal crystal template was obtained by filtration [Supplementary Figure 5][21]. However, HCPOS-1 was not generated in the presence of TSPM and DACH together, and only CPOS-1 with a discrete macropore on the surface was obtained due to the rapid reaction rate [Supplementary Figure 6]. Thus, to further decrease the reaction rate, the PS template was immersed in a methanol solution of DACH, allowing for homogeneous adsorption and dispersion of DACH in the voids, followed by removing methanol to obtain DACH-loaded PS colloidal crystals (denoted as DACH@PS). Next, the DACH@PS was gently placed in the methanol/water solution of TSPM, resulting in the gradual diffusion of TSPM into the voids and reacted with DACH to form CPOS-1 crystals. Finally, the PS template was removed by immersion in THF for 24 h, and the resulting solid was collected, washed with THF, and dried at 150 °C for 8 h to obtain HCPOS-1.

The morphology of both PS colloidal crystal and HCPOS-1 was revealed by SEM. The PS nanospheres are regularly arranged under the driving force of gravity and differential pressure during the filtration[54], forming PS colloidal crystal with an opal structure. As illustrated in Figure 2A and B, the PS colloidal crystal showcases a close-packed face center cubic (FCC) structure, where the formed PS monolayer matches well with the (111) facet of FCC crystal structure and adopts an ABC stacking mode. The PS nanospheres within this PS colloidal crystal possess a uniform size of approximately 250 nm and are densely stacked together to create well-defined voids [Figure 2B]. These voids offer sufficient space for the adsorption of precursors and the synthesis of CPOS-1. HCPOS-1 displays a block-like morphology, boasting an obvious 3D ordered macroporous structure that impeccably complements the PS colloidal crystal template [Figure 2C]. The voids in the original PS colloidal crystal template are completely filled by CPOS-1, forming an anti-opal

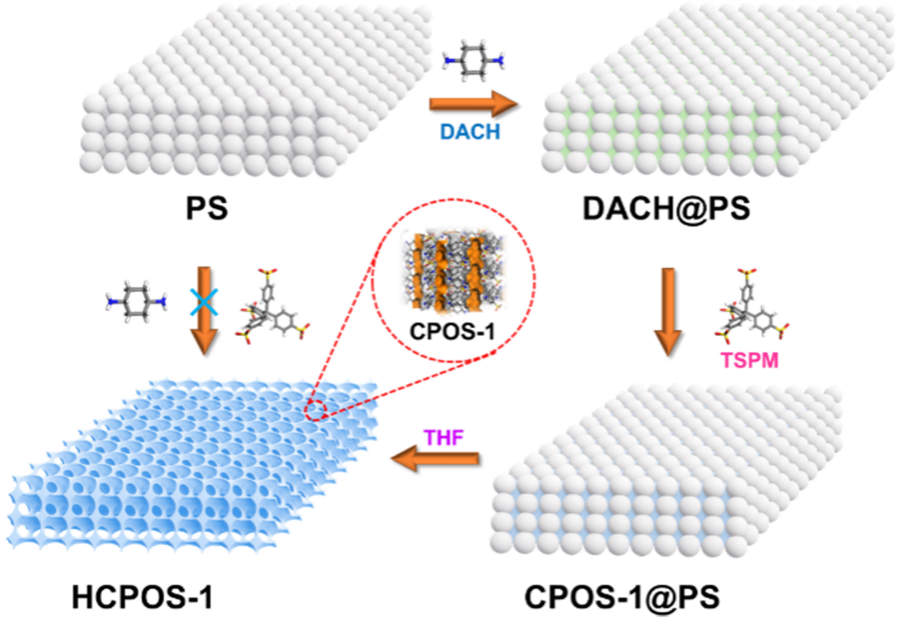

Figure 1. Schematic illustration of the synthesis of 3D ordered macro-/microporous of HCPOS-1. 3D: Three-dimensional; HCPOS: hierarchical crystalline porous organic salt.

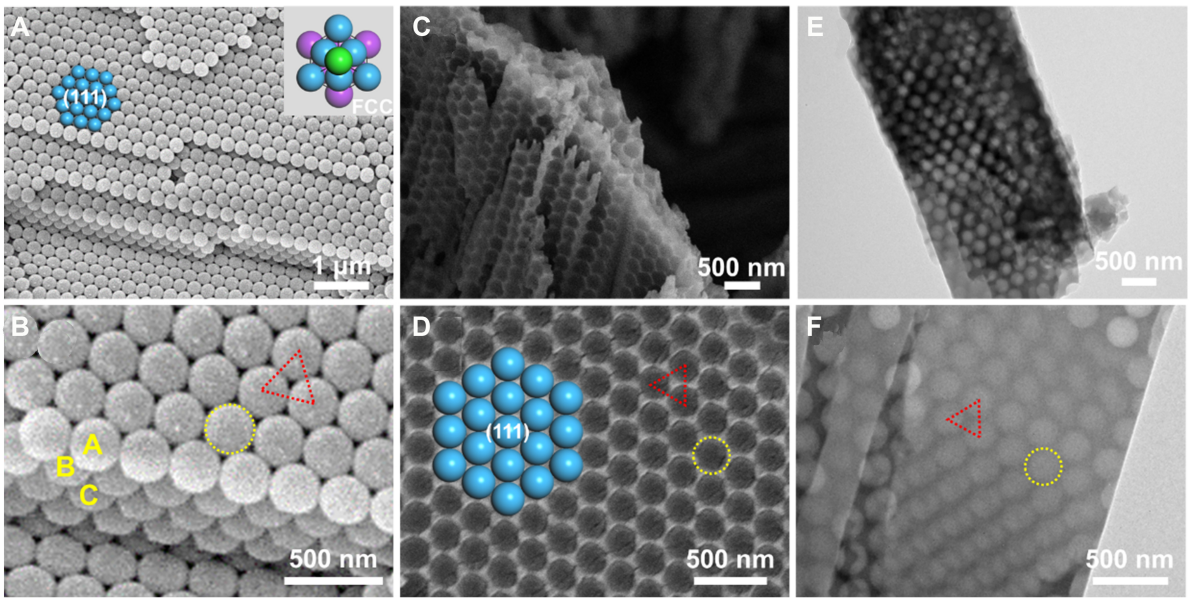

Figure 2. (A) SEM image of PS colloidal crystal template and corresponding FCC crystal structure perpendicular to (111) facet (inset); (B) Zoom-in view of the SEM image, size of PS nanosphere (yellow circle) and voids formed by PS nanospheres (red triangle); (C and D) SEM images of HCPOS-1, size of macropore (yellow cycle) and anti-opal structure formed by CPOS-1 (red triangle); (E and F) TEM images of HCPOS-1, size of macropore (yellow circle) and anti-opal structure formed by CPOS-1 (red triangle). SEM: Scanning electron microscopy; PS: polystyrene; FCC: face center cubic; HCPOS: hierarchical crystalline porous organic salt; CPOS: crystalline porous organic salt; TEM: transmission electron microscopy.

structure upon the removal of the PS template. The regular arrangement of macropores also agrees well with the (111) crystal face in the PS colloid crystal. Additionally, the macropores possess an approximate size of 250 nm, which also aligns well with the size of the PS colloidal crystal template [Figure 2D]. TEM

further confirms the macroporous structure of HCPOS-1. As shown in Figure 2E and F, numerous uniformly arranged and well-ordered macropores within HCPOS-1 are distributed across multiple layers and form a distinct anti-opal structure, which is complementary to the opal structure of PS colloidal crystal template. The diameter of the macropores is approximately 250 nm [Figure 2F], in accordance with the SEM images of HCPOS-1 and the PS colloidal crystal template, further proving the successful preparation of macro-/microporous HCPOS-1.

The PXRD was employed to investigate the crystallinity and phase purity of HCPOS-1 [Figure 3A]. HCPOS-1 exhibits excellent crystallinity, with the PXRD pattern being identical to that of CPOS-1, indicating the preservation of crystalline nature of CPOS-1. Additionally, no excess peaks in PXRD pattern verify the phase purity of HCPOS-1. To further confirm the porous nature of HCPOS-1, CO_2 adsorption experiments were performed at 273 K [Figure 3B]. The CO_2 adsorption capacity of HCPOS-1 is 33.9 $cm^3 \cdot g^{-1}$, similar to that of CPOS-1 (38.9 $cm^3 \cdot g^{-1}$). Subsequently, the pore size distribution of HCPOS-1 was calculated using density functional theory (DFT). The predominant pore size of HCPOS-1 is centered at approximately 5.0 Å [Supplementary Figure 7], which agrees well with the theoretical pore size of CPOS-1 (~5.3 Å, Supplementary Figure 8). These results further support the existence of microporous structures in addition to the 3D ordered macropore in HCPOS-1. FT-IR spectra showcase a broad band at 2,950 cm^{-1} for HCPOS-1, which is associated with the stretching vibrations of primary ammonium cations. Additionally, the bands at 1,593 and 1,537 cm^{-1} correspond to the bending vibrations of primary ammonium cations. The stretching bands at 1,182 and 1,037 cm^{-1} can be attributed to the asymmetric and symmetric stretching of sulfonate anions, respectively [Figure 3C]. These results are consistent with the FT-IR spectrum of CPOS-1, indicating the retention of CPOS-1 structure during the synthesis. Additionally, HCPOS-1 exhibits a thermal stability up to 320 °C, showing no significant differences in TGA plot compared to CPOS-1 [Figure 3D]. Thus, it can be inferred that the stability of CPOS-1 remains.

To validate this approach, CPOS-6, synthesized from TSPM and tetrakis(4-amdinophenyl)methane (TAmPM) in a methanol-water mixture, was selected as an additional example for HCPOS synthesis. As shown in Supplementary Figures 9 and 10, both the PXRD pattern and FT-IR spectra show no significant changes, indicating the preservation of the CPOS-6 structure. The SEM image further confirms the successful synthesis of HCPOS-6, displaying distinct macropores with an average diameter of 250 nm [Supplementary Figure 11]. Consequently, this approach proves to be an effective strategy for fabricating other HCPOSs.

To gain further insight into the properties of macropores in HCPOS-1, enzyme immobilization was performed. As we know, the high concentration and toxicity of H_2O_2 can cause undesired damage to normal tissues[55]. CAT, an iron-heme enzyme, plays a crucial role in reducing the H_2O_2 content in the body and catalyzing reactions outside the body[56]. However, the dimensions of CAT (9.7 × 9.2 × 6.7 nm^3) tend to surpass the pore size of microporous materials, presenting a formidable challenge in its immobilization[35]. HCPOS-1, featuring large enough macropore and numerous sulfonic acid and amino functional groups on the surface, can adsorb enzymes through van der Waals forces, ionic interactions and hydrogen bonding[57], making it an ideal platform for CAT immobilization through physical adsorption. This strategy is straightforward and avoids using organic solvents and harsh conditions, thus preserving the activity of enzymes to a maximum.

To evaluate the CAT immobilization performance of HCPOS-1, we employed a simple and effective method. HCPOS-1 was immersed in an aqueous solution of CAT for six hours, forming CAT-loaded HCPOS-1 (denoted as CAT/HCPOS-1, Figure 4A). The immobilization capacity of CAT in HCPOS-1 was

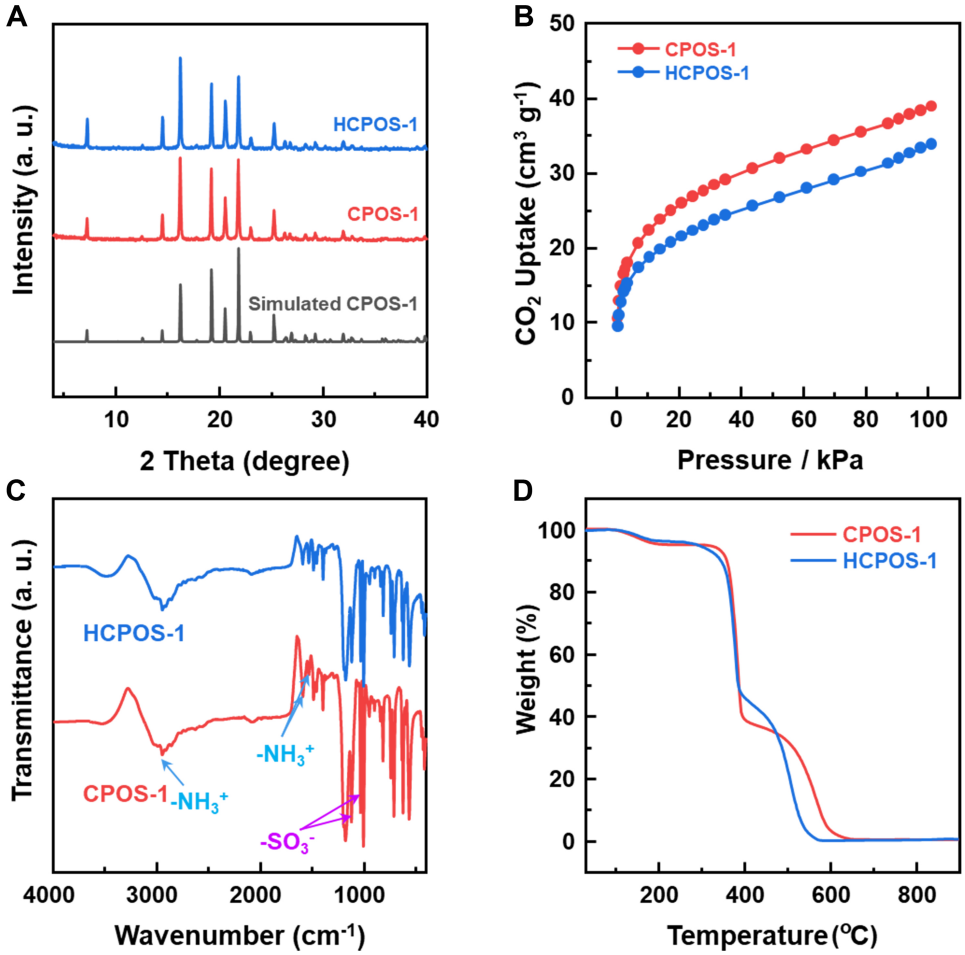

Figure 3. (A) PXRD patterns of HCPOS-1 and CPOS-1; (B) CO_2 sorption isotherms of HCPOS-1 and CPOS-1 at 273 K; (C) FT-IR spectra of HCPOS-1 and CPOS-1; (D) TGA curves of HCPOS-1 and CPOS-1. PXRD: Powder X-ray diffraction; HCPOS: hierarchical crystalline porous organic salt; CPOS: crystalline porous organic salt; FT-IR: Fourier transform infrared; TGA: thermogravimetric analysis.

determined by the Bradford assay [Supplementary Figure 12][50,51]. As illustrated in Figure 4B, the value of immobilization capacity is calculated to be as high as 336.9 mg·g^{-1}, which surpasses that in CPOS-1 (163.3 mg·g^{-1}) and is comparable to other porous organic materials [Supplementary Table 1]. This suggests that the 3D ordered macroporous structure in HCPOS-1 significantly facilitates enzyme diffusion and increases the contact area between enzymes and HCPOS-1, enhancing enzyme immobilization capacity. Subsequently, to assess the distribution of CAT within HCPOS-1, the FCAT was employed for immobilizaiton. The resulting FACT/HCPOS-1 was washed by water to remove the residual FACT on the HCPOS-1 surface. The obvious emission of a homogeneous green fluorescent signal observed in the CLSM image reveals the uniform distribution of FCAT within the macropore of HCPOS-1 [Figure 4C]. The crystallinity of CAT/HCPOS-1 was examined by PXRD and the positions of diffraction peaks show no significant differences with HCPOS-1, demonstrating that the structural integrity of HCPOS-1 remained intact after enzyme immobilization [Figure 4D]. However, a noticeable alteration in the intensity of the PXRD pattern is observed between HCPOS-1 and CAT/HCPOS-1, which can be ascribed to the residual water molecules present within the micropores and the CAT absorbed within the macropores after enzyme immobilization. Furthermore, CO_2 sorption isotherm of CAT/HCPOS-1 displays an uptake of 18.3 cm^3·g^{-1}, lower than that of HCPOS-1 (33.9 cm^3·g^{-1}), further confirming the successful immobilization of CAT [Supplementary Figure 13].

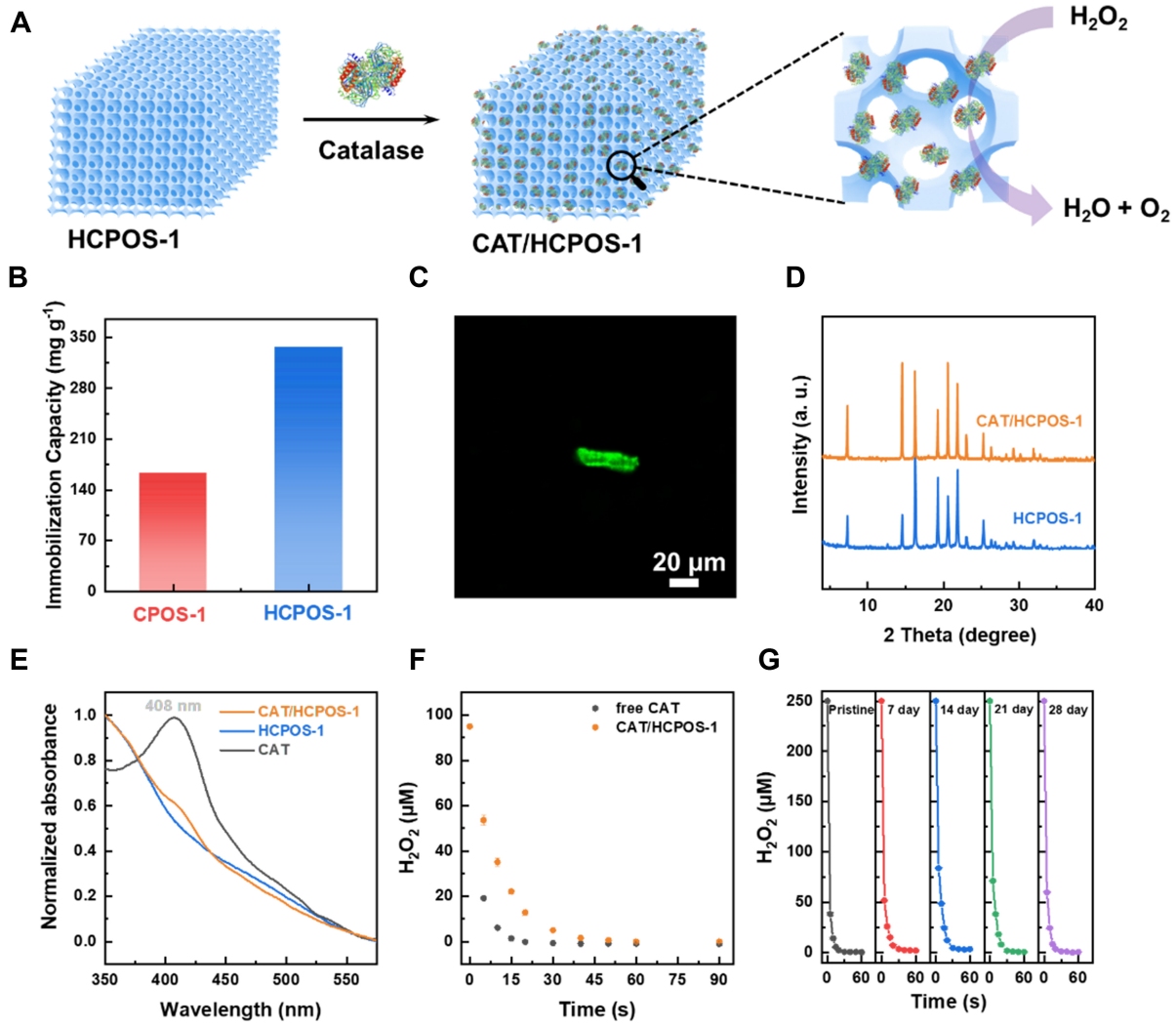

Figure 4. (A) Immobilization process of CAT within HCPOS-1 and decomposition process of H_2O_2 catalyzed by CAT/HCPOS-1; (B) Immobilization capacity of HCPOS-1 and CPOS-1; (C) CLSM image of FITC tagged CAT/HCPOS-1; (D) PXRD patterns of CAT/HCPOS-1 and HCPOS-1; (E) Solid state UV-vis spectra of CAT/HCPOS-1, HCPOS-1 and CAT; (F) Catalytic performance of CAT/HCPOS-1 and free CAT; (G) Storage stability of CAT/HCPOS-1. CAT: Catalase; HCPOS: hierarchical crystalline porous organic salt; CPOS: crystalline porous organic salt; CLSM: confocal laser scanning microscopy; FITC: fluorescein isothiocyanate; PXRD: powder X-ray diffraction; UV-vis: ultraviolet-visible.

The FT-IR spectrum of CAT/HCPOS-1 shows a new stretching band at 1,700-1,600 cm^{-1} corresponding to the amide I region of CAT [Supplementary Figure 14], demonstrating that the presence of CAT within HCPOS-1 and the secondary structure of CAT has no obvious change. The new absorption peak at 408 nm in the solid-state UV-vis spectrum [Figure 4E and Supplementary Figure 15] is attributed to the Soret absorption band (π-π^*) due to the iron-heme cofactor in CAT[58]. Moreover, the similarity in the Soret absorption peaks between free CAT and CAT/HCPOS-1 indicates that the immobilization process does not induce any significant changes in the active site of CAT[59]. CD spectra of free and recovered CAT show no significant change, indicating that the primary conformation is preserved during the immobilization process [Supplementary Figure 16].

The coexistence of microporous and macroporous structures within HCPOS-1 endows it with a large surface area and reduced mass transfer resistance, which are beneficial for enzyme catalysis. Subsequently, the catalytic activity of CAT/HCPOS-1 for the decomposition of H_2O_2 was investigated. FOX reagent was used to determine the concentration of H_2O_2 [Supplementary Figure 17][52,53]. Figure 4F reveals the remarkable catalytic activity of CAT/HCPOS-1 with a rate of 6.0 $\mu M \cdot s^{-1}$, approximately 67% of the activity of the free enzyme (8.9 $\mu M \cdot s^{-1}$), indicating that the enzyme structure is not significantly disrupted during the immobilization process. The hydrophilic nature of the surface plays a crucial role in maintaining the active conformation of enzymes[60,61]. In the case of HCPOS-1, numerous polar functional groups on the surface impart HCPOS-1 with a hydrophilic surface, as confirmed by water contact angle measurement [Supplementary Figure 18]. This hydrophilic environment ensures the preservation of the enzyme conformation, ultimately leading to the remarkable activity observed in CAT/HCPOS-1. To further confirm the influence of the hydrophilic surface on the activity of the enzyme, ZIF-8 with a hydrophobic surface was synthesized for comparison. ZIF-8 showcases uniform dodecahedron morphology with a size of ~2 μm [Supplementary Figure 19]. Subsequently, CAT was also immobilized on the surface of ZIF-8 by physical adsorption [Supplementary Figures 20-22]. However, the immobilization capacity is lower, 31.7 $mg \cdot g^{-1}$, compared to that of HCPOS-1 [Supplementary Figure 23]. The catalytic activity of CAT/ZIF-8 is estimated to be 2.7 $\mu M \cdot s^{-1}$ [Supplementary Figure 24], also lower than that of CAT/HCPOS-1, further demonstrating the advantages of a hydrophilic surface in preserving enzyme conformation. Subsequently, CAT/HCPOS-1 was stored at -20 °C to explore the storage stability [Figure 4G]. After seven days, there is no significant change in catalytic activity, and even after 28 days, it still maintains an excellent catalytic activity for the decomposition of H_2O_2, indicating the stability of CAT/HCPOS-1. Subsequently, the catalytic stability of CAT/HCPOS-1 was investigated. Unfortunately, CAT/HCPOS-1 exhibits a loss of activity after one cycle of catalysis [Supplementary Figure 25]. It can be attributed to the detachment of CAT from HCPOS-1 during the catalytic reaction process, which also confirms the weak interactions between CAT and HCPOS-1 are not strong enough to retain the CAT within HCPOS-1. On the other hand, these results also indicate that CAT can be easily released, which is advantageous for its application in enzyme delivery.

CONCLUSIONS

In summary, a template-assisted approach has been used to fabricate HCPOSs for the first time. CPOS-1, with a hierarchical porous structure, has been successfully synthesized in the presence of a PS colloid crystal template. HCPOS-1 exhibits 3D ordered macroporous and microporous structures. The 3D ordered macroporous structure in HCPOS-1 greatly enhances the diffusion of enzymes and increases the contact area for enzyme immobilization. Consequently, HCPOS-1 exhibits an impressive capacity for immobilizing the CAT enzyme, up to 336.9 $mg \cdot g^{-1}$. Furthermore, the hydrophilic surface of HCPOS-1 avoids the drastic conformation changes of CAT during the immobilization process, endowing CAT/HCPOS-1 with high catalytic activity. Our results provide a highly effective strategy for constructing hierarchical CPOSs specifically designed to immobilize large-sized enzymes. This current work also offers valuable insights for immobilizing other biomacromolecules, viruses, and even cells, thus opening up new avenues for future research in this field.

DECLARATIONS

Authors' contributions

Conceived the idea and led the project: Su BL, Ben T
Designed the samples and performed experiments: Wang J, Xing G
Analyzed the data and wrote the paper: Wang J, Xing G, Chen LH, Zhu W, Su BL, Ben T
Gave the experimental guidance and advice: Zhao Y, Zhou J, Song B, Chen LH, Zhu W

All authors contributed to the general discussion.

Availability of data and materials

The detailed materials and methods in the experiment were listed in the Supplementary Materials. Other raw data that support the findings of this study are available from the corresponding author upon reasonable request.

Financial support and sponsorship

This study was supported by the National Key R&D Program of China (2021YFA1200400), the National Natural Science Foundation of China (No. 91956108, No. 22001191), and the Natural Science Foundation of Zhejiang Province (No. LZ22B010001).

Conflicts of interest

Ben T and Chen LH are Junior Editorial Board members of *Chemical Synthesis*, and Su BL is Editor-in-Chief of *Chemical Synthesis*. The other authors declare that there are no conflicts of interest.

Ethical approval and consent to participate

Not applicable.

Consent for publication

Not applicable.

REFERENCES

1. Xing G, Peng D, Ben T. Crystalline porous organic salts. *Chem Soc Rev* 2024;53:1495-513. DOI PubMed
2. Yu S, Xing GL, Chen LH, Ben T, Su BL. Crystalline porous organic salts: from micropore to hierarchical pores. *Adv Mater* 2020;32:e2003270. DOI PubMed
3. Xing G, Yan T, Das S, Ben T, Qiu S. Synthesis of crystalline porous organic salts with high proton conductivity. *Angew Chem Int Ed Engl* 2018;57:5345-9. DOI PubMed
4. Xing G, Bassanetti I, Bracco S, et al. A double helix of opposite charges to form channels with unique CO_2 selectivity and dynamics. *Chem Sci* 2019;10:730-6. DOI PubMed PMC
5. Zhao Y, Fan C, Pei C, et al. Colossal negative linear compressibility in porous organic salts. *J Am Chem Soc* 2020;142:3593-9. DOI PubMed
6. Zhang S, Fu J, Das S, Ye K, Zhu W, Ben T. Crystalline porous organic salt for ultrarapid adsorption/desorption-based atmospheric water harvesting by dual hydrogen bond system. *Angew Chem Int Ed Engl* 2022;61:e202208660. DOI PubMed
7. Xing G, Zhang S, Zhu W, Ben T. Reply to the correspondence on "Crystalline porous organic salt for ultrarapid adsorption/desorption-based atmospheric water harvesting by dual hydrogen bond system". *Angew Chem Int Ed Engl* 2023;62:e202215074. DOI PubMed
8. Yamamoto A, Hirukawa T, Hisaki I, Miyata M, Tohnai N. Multifunctionalized porosity in zeolitic diamondoid porous organic salt: selective adsorption and guest-responsive fluorescent properties. *Tetrahedron Lett* 2013;54:1268-73. DOI
9. Ami T, Oka K, Tsuchiya K, Tohnai N. Porous organic salts: diversifying void structures and environments. *Angew Chem Int Ed Engl* 2022;61:e202202597. DOI PubMed
10. Sei H, Oka K, Sotome H, Miyasaka H, Tohnai N. Cage-like sodalite-type porous organic salts enabling luminescent molecule's incorporation and room-temperature phosphorescence induction in air. *Small* 2023;19:e2301887. DOI PubMed
11. Brekalo I, Deliz DE, Barbour LJ, Ward MD, Friščić T, Holman KT. Microporosity of a guanidinium organodisulfonate hydrogen-bonded framework. *Angew Chem Int Ed Engl* 2020;59:1997-2002. DOI PubMed
12. O'Shaughnessy M, Padgham AC, Clowes R, et al. Controlling the crystallisation and hydration state of crystalline porous organic salts. *Chemistry* 2023;29:e202302420. DOI PubMed PMC
13. Karmakar A, Illathvalappil R, Anothumakkool B, et al. Hydrogen-bonded organic frameworks (HOFs): a new class of porous crystalline proton-conducting materials. *Angew Chem Int Ed Engl* 2016;55:10667-71. DOI PubMed
14. Comotti A, Bracco S, Yamamoto A, et al. Engineering switchable rotors in molecular crystals with open porosity. *J Am Chem Soc* 2014;136:618-21. DOI PubMed
15. Bracco S, Miyano T, Negroni M, et al. CO_2 regulates molecular rotor dynamics in porous materials. *Chem Commun* 2017;53:7776-9. DOI PubMed
16. Chen LH, Li Y, Su BL. Hierarchy in materials for maximized efficiency. *Natl Sci Rev* 2020;7:1626-30. DOI PubMed PMC

17. Chen LH, Sun MH, Wang Z, Yang W, Xie Z, Su BL. Hierarchically structured zeolites: from design to application. *Chem Rev* 2020;120:11194-294. DOI PubMed
18. Zhou J, Fan W, Wang Y, Xie Z. The essential mass transfer step in hierarchical/nano zeolite: surface diffusion. *Natl Sci Rev* 2020;7:1630-2. DOI PubMed PMC
19. Stein A, Wilson BE, Rudisill SG. Design and functionality of colloidal-crystal-templated materials--chemical applications of inverse opals. *Chem Soc Rev* 2013;42:2763-803. DOI PubMed
20. Li P, Chen Q, Wang TC, et al. Hierarchically engineered mesoporous metal-organic frameworks toward cell-free immobilized enzyme systems. *Chem* 2018;4:1022-34. DOI
21. Shen K, Zhang L, Chen X, et al. Ordered macro-microporous metal-organic framework single crystals. *Science* 2018;359:206-10. DOI PubMed
22. Sun M, Zhou J, Hu Z, et al. Hierarchical zeolite single-crystal reactor for excellent catalytic efficiency. *Matter* 2020;3:1226-45. DOI
23. Yao W, Chen J, Wang Y, et al. Nitrogen-doped carbon composites with ordered macropores and hollow walls. *Angew Chem Int Ed Engl* 2021;60:23729-34. DOI PubMed
24. Yao W, Hu C, Zhang Y, et al. Hierarchically ordered porous carbon with atomically dispersed cobalt for oxidative esterification of furfural. *Ind Chem Mater* 2023;1:106-16. DOI
25. Zhao X, Pachfule P, Li S, et al. Macro/microporous covalent organic frameworks for efficient electrocatalysis. *J Am Chem Soc* 2019;141:6623-30. DOI PubMed
26. Liu T, Zhao Y, Song M, et al. Ordered macro-microporous single crystals of covalent organic frameworks with efficient sorption of iodine. *J Am Chem Soc* 2023;145:2544-52. DOI PubMed
27. Schoemaker HE, Mink D, Wubbolts MG. Dispelling the myths - biocatalysis in industrial synthesis. *Science* 2003;299:1694-7. DOI PubMed
28. Straathof AJJ. Transformation of biomass into commodity chemicals using enzymes or cells. *Chem Rev* 2014;114:1871-908. DOI PubMed
29. Liang W, Wied P, Carraro F, et al. Metal-organic framework-based enzyme biocomposites. *Chem Rev* 2021;121:1077-129. DOI PubMed
30. Huang S, Chen G, Ouyang G. Confining enzymes in porous organic frameworks: from synthetic strategy and characterization to healthcare applications. *Chem Soc Rev* 2022;51:6824-63. DOI PubMed
31. Chen W, Vázquez-gonzález M, Zoabi A, Abu-reziq R, Willner I. Biocatalytic cascades driven by enzymes encapsulated in metal–organic framework nanoparticles. *Nat Catal* 2018;1:689-95. DOI
32. An H, Song J, Wang T, et al. Metal-organic framework disintegrants: enzyme preparation platforms with boosted activity. *Angew Chem Int Ed Engl* 2020;59:16764-9. DOI PubMed
33. Lu J, Wu JK, Jiang Y, et al. Fabrication of microporous metal-organic frameworks in uninterrupted mesoporous tunnels: hierarchical structure for efficient trypsin immobilization and stabilization. *Angew Chem Int Ed Engl* 2020;59:6428-34. DOI PubMed
34. Liang J, Bin Zulkifli MY, Yong J, et al. Locking the ultrasound-induced active conformation of metalloenzymes in metal-organic frameworks. *J Am Chem Soc* 2022;144:17865-75. DOI PubMed
35. Tang J, Liu J, Zheng Q, et al. In-situ encapsulation of protein into nanoscale hydrogen-bonded organic frameworks for intracellular biocatalysis. *Angew Chem Int Ed Engl* 2021;60:22315-21. DOI PubMed
36. Chen G, Huang S, Shen Y, et al. Protein-directed, hydrogen-bonded biohybrid framework. *Chem* 2021;7:2722-42. DOI
37. Wied P, Carraro F, Bolivar JM, Doonan CJ, Falcaro P, Nidetzky B. Combining a genetically engineered oxidase with hydrogen-bonded organic frameworks (HOFs) for highly efficient biocomposites. *Angew Chem Int Ed Engl* 2022;61:e202117345. DOI PubMed PMC
38. Chen G, Tong L, Huang S, Huang S, Zhu F, Ouyang G. Hydrogen-bonded organic framework biomimetic entrapment allowing non-native biocatalytic activity in enzyme. *Nat Commun* 2022;13:4816. DOI PubMed PMC
39. Xing C, Mei P, Mu Z, et al. Enhancing enzyme activity by the modulation of covalent interactions in the confined channels of covalent organic frameworks. *Angew Chem Int Ed Engl* 2022;61:e202201378. DOI PubMed
40. Feng M, Niu Z, Xing C, et al. Covalent organic framework based crosslinked porous microcapsules for enzymatic catalysis. *Angew Chem Int Ed Engl* 2023;62:e202306621. DOI PubMed
41. Liang J, Ruan J, Njegic B, et al. Insight into bioactivity of in-situ trapped enzyme-covalent-organic frameworks. *Angew Chem Int Ed Engl* 2023;62:e202303001. DOI PubMed
42. Zhang Y, Xing C, Mu Z, et al. Harnessing self-repairing and crystallization processes for effective enzyme encapsulation in covalent organic frameworks. *J Am Chem Soc* 2023;145:13469-75. DOI PubMed
43. Liu H, Zhou Y, Guo J, et al. Reticular synthesis of highly crystalline three-dimensional mesoporous covalent-organic frameworks for lipase inclusion. *J Am Chem Soc* 2023;145:23227-37. DOI PubMed
44. Liu S, Sun Y. Co-encapsulating cofactor and enzymes in hydrogen-bonded organic frameworks for multienzyme cascade reactions with cofactor recycling. *Angew Chem Int Ed Engl* 2023;62:e202308562. DOI PubMed
45. Freund R, Zaremba O, Arnauts G, et al. The current status of MOF and COF applications. *Angew Chem Int Ed Engl* 2021;60:23975-4001. DOI PubMed
46. Kandambeth S, Venkatesh V, Shinde DB, et al. Self-templated chemically stable hollow spherical covalent organic framework. *Nat Commun* 2015;6:6786. DOI PubMed

47. Sun Q, Fu CW, Aguila B, et al. Pore environment control and enhanced performance of enzymes infiltrated in covalent organic frameworks. *J Am Chem Soc* 2018;140:984-92. DOI PubMed
48. Liang W, Ricco R, Maddigan NK, et al. Control of structure topology and spatial distribution of biomacromolecules in protein@ZIF-8 biocomposites. *Chem Mater* 2018;30:1069-77. DOI
49. Feng Y, Hu H, Wang Z, et al. Three-dimensional ordered magnetic macroporous metal-organic frameworks for enzyme immobilization. *J Colloid Interface Sci* 2021;590:436-45. DOI PubMed
50. Bradford MM. A rapid and sensitive method for the quantitation of microgram quantities of protein utilizing the principle of protein-dye binding. *Anal Biochem* 1976;72:248-54. DOI PubMed
51. Liang W, Flint K, Yao Y, et al. Enhanced bioactivity of enzyme/MOF biocomposite via host framework engineering. *J Am Chem Soc* 2023;145:20365-74. DOI PubMed
52. Ou P, Wolff SP. A discontinuous method for catalase determination at 'near physiological' concentrations of H_2O_2 and its application to the study of H_2O_2 fluxes within cells. *J Biochem Biophys Methods* 1996;31:59-67. DOI PubMed
53. Li M, Qiao S, Zheng Y, et al. Fabricating covalent organic framework capsules with commodious microenvironment for enzymes. *J Am Chem Soc* 2020;142:6675-81. DOI PubMed
54. Stein A, Schroden RC. Colloidal crystal templating of three-dimensionally ordered macroporous solids: materials for photonics and beyond. *Curr Opin Solid St M* 2001;5:553-64. DOI
55. Liu X, Yan Z, Zhang Y, et al. Two-dimensional metal-organic framework/enzyme hybrid nanocatalyst as a benign and self-activated cascade reagent for *in vivo* wound healing. *ACS Nano* 2019;13:5222-30. DOI PubMed
56. Fita I, Rossmann MG. The NADPH binding site on beef liver catalase. *Proc Natl Acad Sci U S A* 1985;82:1604-8. DOI PubMed PMC
57. Jesionowski T, Zdarta J, Krajewska B. Enzyme immobilization by adsorption: a review. *Adsorption* 2014;20:801-21. DOI
58. Liang W, Carraro F, Solomon MB, et al. Enzyme encapsulation in a porous hydrogen-bonded organic framework. *J Am Chem Soc* 2019;141:14298-305. DOI PubMed
59. Dong X, Fan Y, Yang P, et al. Ultraviolet-visible (UV-Vis) and fluorescence spectroscopic investigation of the interactions of ionic liquids and catalase. *Appl Spectrosc* 2016;70:1851-60. DOI PubMed
60. Liang W, Xu H, Carraro F, et al. Enhanced activity of enzymes encapsulated in hydrophilic metal-organic frameworks. *J Am Chem Soc* 2019;141:2348-55. DOI PubMed
61. Pan Y, Wang X, Li H, et al. In situ monitoring of protein transfer into nanoscale channels. *Cell Rep Phys Sci* 2021;2:100576. DOI